Battery health prognostic with sensor-free differential temperature voltammetry reconstruction and capacity estimation based on multi-domain adaptation

Che, Yunhong; Vilsen, Søren Byg; Meng, Jinhao; Sui, Xin; Teodorescu, Remus

Published in:
eTransportation

DOI (link to publication from Publisher):
10.1016/j.etran.2023.100245

Publication date:
2023

Document Version
Publisher's PDF, also known as Version of record

eTransportation 17 (2023) 100245

Contents lists available at ScienceDirect

eTransportation

journal homepage: www.journals.elsevier.com/etransportation

Battery health prognostic with sensor-free differential temperature voltammetry reconstruction and capacity estimation based on multi-domain adaptation

Yunhong Che [a,c], Søren Byg Vilsen [a,d], Jinhao Meng [b,*], Xin Sui [a,**], Remus Teodorescu [a]

[a] Department of Energy, Aalborg University, 9220, Aalborg, Denmark
[b] School of Electrical Engineering, Xi'an Jiaotong University, Xi'an, 710049, PR China
[c] Laboratory of Intelligent Maintenance and Operations Systems, EPFL, 1015 Lausanne, Switzerland
[d] Department of Mathematical Sciences, Aalborg University, Aalborg, 9220, Denmark

ARTICLE INFO

Keywords:
Battery health prognostic
State of health estimation
Differential temperature voltammetry
Domain adaptation
Transfer learning

ABSTRACT

Battery health prognostic is a key part of battery management used to ensure safe and optimal usage. A novel method for end-to-end sensor-free differential temperature voltammetry reconstruction and state of health estimation based on the multi-domain adaptation is proposed in this paper. Firstly, the partial charging or discharging curve is used to reconstruct the differential temperature curve, removing the requirement for the temperature sensor measurement. The partial differential capacity curve and the reconstructed differential temperature curve are input and then used in an end-to-end state of health estimation. Finally, to reduce the domain discrepancy between the source and target domains, the maximum mean discrepancy is included as an additional loss to improve the accuracy of both differential temperature curve reconstruction and state of health estimation with unlabeled data from the testing battery. Four data sets containing both experimental data and public data with different battery chemistry and formats, current modes and rates, and external conditions are used for the verification and evaluation. Experimental results indicate the proposed method can satisfy health prognostics under different scenarios with mean errors of less than 0.067 °C/V for differential temperature curves and 1.78% for the state of health. The results show that the error for the differential temperature curve reconstruction is reduced by more than 20% and the error for the state of health estimation is reduced by more than 47% of the proposed method compared to the conventional data-driven method without transfer learning.

1. Introduction

1.1. Background

The electrification of transportation such as electric vehicles, electric ships, and electric aircraft has developed rapidly in recent years, where lithium-ion batteries serve as the main energy storage devices that benefit from their high energy and power density, low self-discharge rate, and long lifespan [1]. However, due to the side reactions that occurred along with the charging and discharging cycles, the batteries degrade with usage [2], which influences serviceability, reliability, and safety. The health prognostics of the battery are essential for the battery management system (BMS) to guide predictive maintenance that avoids abusive usage, ensures reliable and safe operation, and extends the lifetime [3]. Besides health estimation and prediction, thermal estimation is important to reflect the safety status of the batteries, especially in sensor-free conditions, as a tool for developing thermal runaway warning strategies [4]. Therefore, the temperature variation and current capacity are key information for the prognostics of battery health. Unfortunately, the capacity cannot be measured directly and temperature sensors are not implemented on every battery in real applications. Therefore, advanced methods for indirect assessment of battery health are required, which becomes a hot topic in battery management recently for researchers [5]. Besides, artificial intelligence develops rapidly in recent years, which provides more opportunities for smarter battery management [6]. Inspired by the main interest of both academia and industry, this paper focuses on battery health prognostics with differential temperature (DT or *dT*) elementary reconstruction and state of

* Corresponding author.
** Corresponding author.
E-mail addresses: jinhao@xjtu.edu.cn (J. Meng), xin@energy.aau.dk (X. Sui).

https://doi.org/10.1016/j.etran.2023.100245
Received 22 September 2022; Received in revised form 25 February 2023; Accepted 6 April 2023
Available online 7 April 2023

health (SoH) estimation for energy storage systems using unlabeled aging data and without temperature measurement based on novel transfer learning strategies.

1.2. Literature review

Model-based and data-driven are the two main categories in battery state estimation and health prognostics. Model-based method generally first builds electrochemical models to capture the electrical/thermal characteristics of batteries [7,8]. Then, the parameter estimation method based on various optimization algorithms is conducted for state estimations and health prognostics [9,10]. Nevertheless, the high complexity and computation burden make it challenging for the practical implementation of model-based methods. On the other hand, data-driven methods are more flexible, easier to implement, can avoid those complex modeling processes, etc. [11], which attracts more and more concerns in recent years.

SoH, which is defined as the ratio of the current capacity to the nominal capacity (or the capacity of the fresh cell), is one key index to evaluate the health status and aging condition of the battery [12]. Data-driven battery SoH estimation can be divided into feature based-methods and feature-free methods. In the feature-based method, manual health indicator (HI) extraction and selection are required [13]. Methods for HI extraction can be divided into measured data-based extraction and calculated data-based extraction. In the measured data-based method, as the voltage, current, and time are recorded online by the BMS, the HIs could be extracted from these data [14]. For example, the widely used time interval during certain voltage ranges, voltage slope, voltage skewness, etc. [15], based HIs have shown satisfactory correlations with battery SoH and helped estimate SoH accurately with machine learning algorithms, such as linear/multi-linear regression, support vector regression, and gaussian process regression, etc. [16–18]. In addition to the direct HIs extraction from the measured data, another way to extract the HIs from parameters such as the incremental capacity (IC) and differential voltage (DV) [19]. The peak values, valley values, and peak areas of IC and DV curves are widely used HIs. Besides, the DT curve has also been proven to reflect battery aging and could help improve the accuracy of SoH estimation along with the IC curve [20]. After the HIs have been extracted, the feature selection process is required to select the most relevant HIs as the final input of the data-driven model. The most popular way is to calculate the correlation coefficients between the HIs and the capacity to help find HIs which are highly correlated with battery capacity [21]. Published works have proven that the wrapper and fusion-based feature selection methods could also help reduce the feature redundancy to help improve the SoH estimation [22]. In the feature-based method, the HI extraction and selection processes are the key steps affecting the final prognostic performance. On the other hand, in feature-free based methods, the raw measurement data is used as input for machine learning or deep learning models directly [23]. A popular feature-free method is to use an auto-encoder and -decoder for automatic feature extraction, with two of the more widely used types of encoder and decoder being recurrent neural networks and convolutional neural networks due to their ability to account for time and spatial dimensions [24–26]. Based on the deep learning method, the battery SoH can be estimated without manual feature engineering [27]. For example, the hybrid network combining convolutional module, ultra-lightweight subspace attention mechanism module, and recurrent unit module was used for decoding with partial charging curve as input while the simple back propagation neural network was used to decode the hidden states for battery SoH estimations [28].

The trained data-driven model mapping the relationship between the input HIs or measured data and battery SoH is then used for estimating the SoH of test batteries. However, the specific mapping might not be suitable for different operation scenarios, where the domains have clear discrepancies. Therefore, researchers have proposed transfer learning to improve the model performance on the SoH estimation for test batteries. Two kinds of transfer learning strategies are widely used (1) to retrain the model using only a few labeled data collected from the test batteries [29,30], and (2) to integrate the reduction strategy of domain discrepancy between the training battery and testing battery into the model [31]. In practical applications, it is very difficult to obtain labeled data from the test battery for model improvement. Therefore, methods that only take advantage of the unlabeled data of the test battery to improve the estimation accuracy are significantly more important, which is the main focus of this paper. In addition, batteries undergo variable temperature conditions in practical applications due to environmental variations. SoH estimation verifications of data-driven methods under variable temperatures have not been seen in the existing literature.

In addition to the direct estimation of battery SoH, more aging-related prognostics have been conducted. Tian et al. [27], proposed a novel deep-learning method for the charging curve prediction with only 30 points collected in 10 min under different aging conditions. The effects have been validated with different batteries aging with different current rates and temperatures. They further implemented the deep neural network for the open circuit voltage reconstruction using partial charging data, where the electrode aging parameters can also be obtained directly [32]. Tang et al. [33], proposed an IC curve reconstruction method that ensures effective feature extraction under noisy conditions for battery SoH estimation. Moreover, temperature variation estimation is also important in battery health prognostics. The temperature variation changes with the battery aging [34], seen as e.g., the incremental value of temperature increases with aging. It is vital to estimate the temperature variation accurately, as it helps provide information for thermal management to avoid thermal runaway. Furthermore, the DT curve also provides additional information which can be used to improve the accuracy of SoH estimation as illustrated in Ref. [20]. For the data-driven temperature estimation, the long-short-term memory (LSTM) neural network is used to predict the future surface temperature using historical information including temperature, voltage, current, and state of charge [35]. The temperature variation with battery aging was decomposed as reversible heat and irreversible heat, and the LSTM was used to predict the temperature variations [36]. However, most data-driven temperature estimation or prediction method needs the measured temperature for the input, while not all the cells have a related temperature sensor in the real world. Therefore, the temperature variation needs to be estimated in the context of a temperature sensor-free environment to provide the thermal behavior of a battery. The investigation of the effectiveness of the SoH estimation with additional estimated temperature characteristics is also valuable while lacking in the existing literature.

1.3. Contribution of this work

This paper proposes a proper method for battery health prognostics with *dT* curve reconstruction and SoH estimation to handle the gaps mentioned above. The following main contributions distinguish this paper from existing works.

1) The *dT* curve is reconstructed by using the *Q-V* curve without the requirement of measured temperature to add information in battery health prognostic. The sequence-to-sequence (STS) method is proposed for the *dT* curve reconstruction by using *dQ* curve.
2) An end-to-end framework is proposed for the SoH estimation with measured *dQ-V* and reconstructed *dT-V* information without the requirement of manual feature extraction and selection.
3) Multiple domain adaptation with maximum mean discrepancy (MMD) is proposed to reduce the domain discrepancy between the training battery and test battery to improve the accuracy of the health prognostics. Both the *dT* curve reconstruction and SoH estimation will benefit from this transfer learning framework without labeled data from the test battery.

4) Both experimental data and publicly available data are used for the evaluation of the proposed method, where different battery chemistry and formats, temperature variations, *dT* curve shapes, and capacity degradation patterns are used for the evaluations of the proposed framework.

The health prognostic framework for the STS *dT* curve reconstruction and sequence-to-point (STP) SoH estimation based on the domain adaptative end-to-end framework is shown in Fig. 1. The *Q-V* curve is transformed into *dQ-V* curve (i.e., building the *dQ* sequence) for input into the neural network. The *dT* curve reconstruction network takes the *dQ* sequence as the input, using the LSTM layer for hidden information extraction since the high coupling relationship on the time series data, and finally, a fully connected layer is added to output the predicted *dT* sequence. The MMD loss is added to the output of the second LSTM to reduce the domain discrepancy of the feature distributions between the source battery and the target battery. The estimated *dT* sequence and the *dQ* sequence are then used for the SoH estimation of batteries, where the MMD loss is also integrated after the second LSTM layer to reduce the domain discrepancy before the final output. The proposed health prognostic strategy is finally verified using different batteries working under different scenarios.

1.4. Article organization

The remainder of this paper is arranged as follows: Both the experimental and public datasets for the verification are introduced in section 2. Then, the main framework of the proposed method will be described in section 3. The prognostic results will be presented and evaluated in section 4, and lastly, the main conclusions of the paper are summarized in section 5.

2. Data description

To better demonstrate the effectiveness of the proposed framework, two private experimental datasets and two public datasets are used. Detailed information for all the datasets used in this paper is listed in Table 1.

The private lab data (denoted as Lab dataset #1 and Lab dataset #2 in Table 1) consists of two pouch cells (with a nominal capacity of 8 Ah). In Lab dataset #1, the batteries are aged using a multi-stage fast constant current (MCC) and constant voltage (CV) charging, and dynamic discharging profile. Specifically, batteries were charged with a series MCC (i.e., 10 C-5 C-3 C–1 C in order). The batteries were charged using 10C first until the voltage reaches the upper limit, i.e., 4.2 V. Then the current was reduced to 5C, 3C, and 1C in sequence to charge until 4.2 V. Then CV charging is followed until the current drops below 0.1C. During discharging, 100 A pulses lasting 10 s are used first to discharge the battery, thereby preventing its voltage from varying beyond the upper voltage limit. The battery was then discharged with two dynamic discharging profiles, one is the urban dynamometer driving schedule (UDDS) and another is HWFET tests for the purpose to simulate battery aging under urban driving conditions and highway driving conditions, respectively. Finally, a 50 A current is loaded to discharge the battery until its voltage drops below the lower voltage limit, i.e., 2.75 V. Furthermore, a short rest lasting 120 s was added between the charging and discharging profiles. The load current as well as the corresponding voltage and temperature responses for the cycling profile with UDDS and HWFET are shown in Fig. 2 (a) and Fig. 2 (b), respectively. A fast temperature increase was found in MCC charging, especially in the first stage of the charging process (at 10C). Thus, accurately estimating the *dT* curve during fast MCC is important to avoid thermal runaways, which could have catastrophic consequences in the real world.

As for the second-life batteries (Lab dataset #2), a typical loading profile of CC-CV/CC is used to continue aging the batteries at 2.5C. The load current, corresponding voltage, and measured temperature are plotted in Fig. 1 (c). It can be seen that the temperature mainly increases during the discharging process, which is different from the primary battery aging process. It shows that the temperature variation of the new batteries (i.e., in Lab dataset#1) is larger than 15 °C while that of the second-life batteries (i.e., in Lab dataset#2) is larger than 10 °C. The temperature variation of the new batteries is larger than the second-life batteries because of the larger current rates. This further solidifies the importance of *dT* curve estimation to provide key information for predictive maintenance of the battery cell. In addition, the environmental temperature of the Lab dataset#2 is changeable between 25 and 35-25-15 °C, which will cause discontinuous degradation curves. It is more related to real scenarios where batteries are aged under variable temperature conditions due to climate change, which makes the verification more conformed to practical applications.

For the public dataset, the data sets from Oxford university [37] (Ox dataset) and MIT-Stanford group [38] (M − S dataset) were used. Detailed information is listed in Table 1. The Ox dataset also uses the pouch cell but with a much smaller current rate and different nominal capacity from the Lab datasets. The M − S dataset uses a large current rate but has different battery chemistry and format from the Lab datasets. It is worth mentioning that the used four datasets cover different scenarios including battery chemistries (i.e., LFP and NCA), battery formats (i.e., pouch and cylindric), and working currents (i.e., high and low current). The large range of operation scenarios, conditions, and chemistries causes large differences in temperature variation and degradation patterns. Therefore, these datasets create a good basis for verifying the robustness and generalization of the proposed framework.

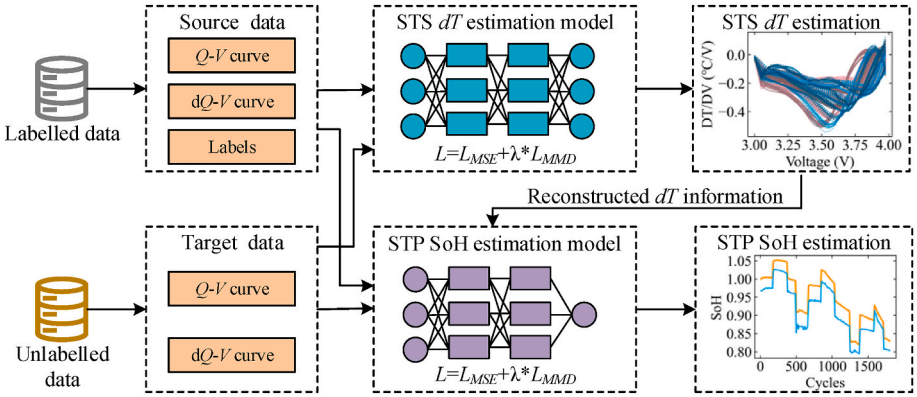

Fig. 1. Framework for domain adaptative battery health prognostics with *dT* curve reconstruction and SoH estimation.

Table 1
Specifications of the data sets used in this paper.

Dataset	Battery Chemistry	Battery Format	Charging/Discharging Profile	Temperature Variation	Environmental Temperature
Lab dataset #1	NCA/Graphite	Pouch	MCC CV/Dynamic	>15 °C	25 °C
Lab dataset #2	NCA/Graphite	Pouch	CC-CV/CC	>10 °C	25-35-25-15 °C cyclic
Ox dataset	NCA/Graphite	Pouch	CC-CV	>1.5 °C	40 °C
M − S dataset	LFP/Graphite	Cylindric	MCC-CV/CC	>5 °C	35 °C

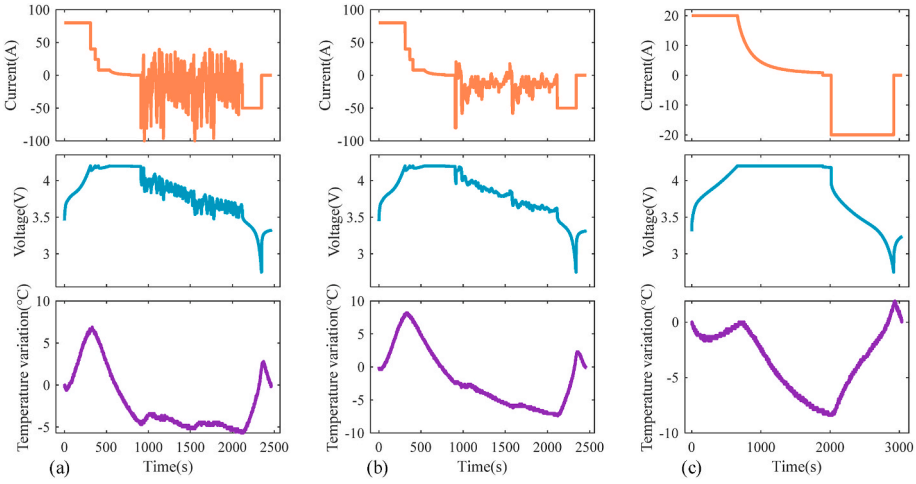

Fig. 2. The loading current and the corresponding voltage and temperature responses under (a) MCC-CV/UDDS work profile, (b) MCC-CV/HWFET work profile, and (c) CC-CV/CC work profile for the second-life battery.

3. Methodology

The detailed methods for the *dT* curve reconstruction and SoH estimation are described in this section. Firstly, the STS framework for *dT* curve reconstruction is introduced in section 3.1. Then, by integrating the *dQ* sequence and the reconstructed dT sequence, the STP-based battery SoH estimation is described in section 3.2. Finally, the domain adaptation for performance improvement via unlabeled data is proposed in section 3.3.

3.1. DT curve reconstruction

The *dT* curve reconstruction is achieved by an STS prediction framework. The input and output of the deep learning model are the *dQ* sequence and *dT* sequence, respectively. The following steps are used to form the *dQ* sequence and *dT* sequence. When the *dQ* sequence is constructed, the voltage is required to pass through a certain voltage range to ensure homogeneity. Thus, *Q-V* curve is chosen to be in the voltage range [3.2 V, 3.6 V] for LFP battery and [3.6 V, 4.2 V] for NCA battery

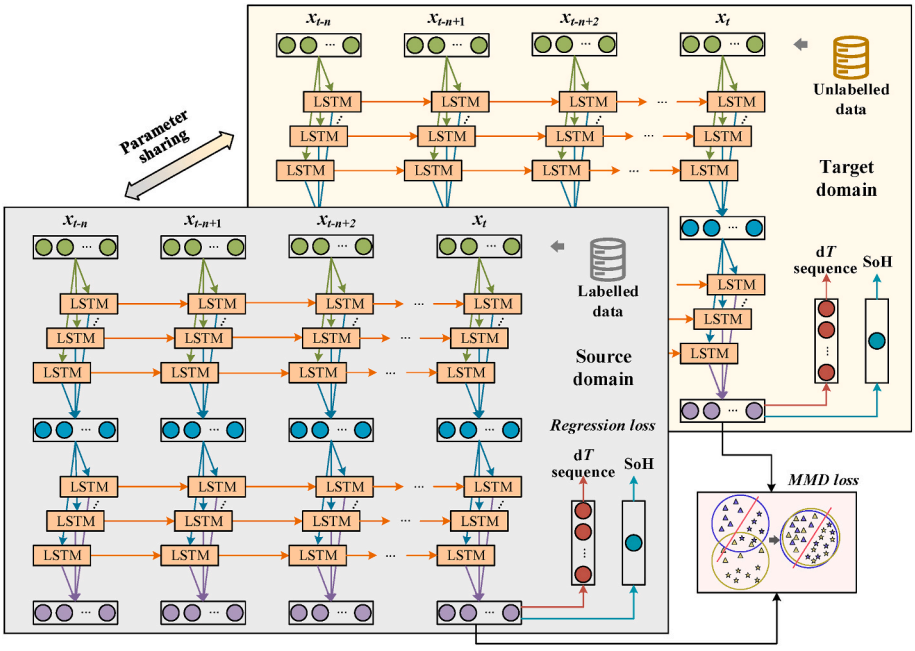

Fig. 3. The structure of the network for the STS *dT* curve reconstruction and STP SoH estimation with domain adaptation.

during primary life and [3.0V, 4.0 V] for the second life battery (i.e. Lab dataset#2). For the Oxford dataset, the whole voltage range is used to demonstrate the whole dT curve variation under a small current rate. The different voltage ranges can also be used to demonstrate that the proposed method could work with both different partial and full Q-V data with these different settings. Then, a predefined voltage interval (0.025V in this paper) is used to split the V sequence and a new Q sequence is obtained by interpolating the Q-V curve based on the split V sequence. Finally, the dQ sequence could be calculated by the difference between each element and the first value in the Q sequence. The same process is used for pre-processing the T-V curve to obtain the dT sequence.

The neural network used for the end-to-end STS dT curve reconstruction is shown in Fig. 3, where the LSTM layer is used for hidden information extraction. LSTM has been widely used in battery SOH estimation and prediction and has proven to be superior in health prognostic [39]. The basic equations governing an LSTM cell are denoted as follows [40].

$$f(t)=\sigma\left(w_{f1}x(t)+w_{f2}h(t-1)+b_f\right) \tag{1}$$

$$i(t)=\sigma(w_{i1}x(t)+w_{i2}h(t-1)+b_i) \tag{2}$$

$$\widetilde{S}(t)=tanh(w_{c1}x(t)+w_{c2}h(t-1)+b_c) \tag{3}$$

$$S(t)=f(t)\odot S(t-1)+i(t)\odot\widetilde{S}(t) \tag{4}$$

$$o(t)=\sigma(w_{o1}x(t)+w_{o2}h(t-1)+b_o) \tag{5}$$

$$h(t)=o(t)\odot\tanh\left(S(t)\right) \tag{6}$$

where $x(t)$ and $h(t)$ are the input and output, $S(t)$ is the state information, $f(t)$, $i(t)$, and $o(t)$ are the information updated by the forget gate, input gate, and output gate respectively, w and b are the weights and biases, σ and tanh are the activation functions.

After the second LSTM, a fully connected layer is added to output the estimated dT sequence. The numbers of neurons used in the two LSTM layers are set to 50 and 30, respectively. Since the dT curve is estimated by inputting the dQ sequence, and the sequences are obtained by splitting the corresponding curves with the same voltage sequence, the output length is the same as the input.

3.2. End-to-end SoH estimation

After reconstructing the dT curve, the temperature variation information is added together with the dQ curve for the end-to-end STP SoH estimation. Specifically, the dQ sequence is selected as one input dimension. In addition, the information from the temperature variation also contains important aging information and helps improve the SoH estimation accuracy, which is proved in the previous study [20]. Therefore, the reconstructed dT curve is added as a second input dimension to the deep learning model. The definition of SoH in this paper is the ratio of the current test capacity (C_i) and the capacity of the first cycle (C_0) [41,42], which is given below.

$$SOH=C_i/C_0 \tag{7}$$

The structure of the neural network for the STP SoH estimation is shown in Fig. 3. It follows the same general structure as the deep neural network used for the dT curve reconstruction, two LSTM layers are first used to extract the hidden aging information. Then, a fully connected layer with one neuron is added to the output for the final SoH estimation. The hyperparameters are set as the same as the model in dT curve reconstruction instead of the output neuron, which is set as 1 for the SoH estimation.

3.3. Transfer learning with domain adaptation

Deep learning-based battery health prognostics for dT curve reconstruction and SoH estimation have been introduced above. However, conventional data-driven methods suffer from poor generalization, as the model trained on the source battery may have poor performance on a target battery, especially when the application scenarios show obvious dissimilarities. These dissimilarities will cause large domain discrepancies between the source battery and the target battery. In most existing transfer learning-based battery health prognostic methods, a few labeled data from the target domain are used to fine-tune the model. However, the labeled data are generally unavailable in real-world applications. Therefore, it is more valuable to use unlabeled to improve the prognostic accuracy. To this end, this paper adopts the MMD to reduce the domain discrepancy of the hidden features outputted by the second LSTM. The implementation of the MMD in the prognostic model is shown in Fig. 3, where the domain discrepancy of the outputs at the last time step of the second LSTM in the source and target domains is reduced, which helps improve the estimation accuracy of dT curve and SoH.

The MMD is a measure of the difference between two probability distributions in the mean embedding of the features [43]. Given two samples in two datasets $X=\{x_i\}_{i=1}^{n_1}$ and $Y=\{y_i\}_{i=1}^{n_2}$, the MMD between the X and Y could be expressed as [44],

$$MMD_{\mathscr{H}}(X,Y)=sup_{\Phi\in\mathscr{H}}\left(E_p[\Phi(x)]-E_q[\Phi(y)]\right), \tag{8}$$

where $\mathscr{H}$ represents a reproducing kernel Hilbert space (RKHS), $\Phi(\bullet)$ is a nonlinear mapping function from raw data space to the RKHS space, and p and q are the probability distributions of generating the two data sets. The empirical approximation to the MMD can be denoted as follows [31,45],

$$MMD^2_{\mathscr{H}}(X,Y)=\left\|\frac{1}{n_1}\sum_{i=1}^{n_1}\Phi(x_i)-\frac{1}{n_2}\sum_{j=1}^{n_2}\Phi\left(y_j\right)\right\|^2_{\mathscr{H}}. \tag{9}$$

The kernel trick is then used to get the expression [31],

$$MMD^2_{\mathscr{H}}(X,Y)=\frac{1}{n_1^2}\sum_{i=1}^{n_1}\sum_{j=1}^{n_2}k\left(x_i,x_j\right)-\frac{2}{n_1n_2}\sum_{i=1}^{n_1}\sum_{j=1}^{n_2}k\left(x_i,y_j\right)+\frac{1}{n_2^2}\sum_{i=1}^{n_1}\times\sum_{j=1}^{n_2}k\left(y_i,y_j\right), \tag{10}$$

where k(•,•) is the kernel function of the RKHS, where the Gaussian radial basis function (RBF) is used [31],

$$k\left(x_i,y_j\right)=\left(-\left\|x_i-y_j\right\|^2\right)/2\gamma^2. \tag{11}$$

In the training process for both the dT curve reconstruction and SoH estimation, the mean square error is used to evaluate the fitting performance of the output, while the MMD is used as an additional loss to evaluate the domain discrepancy of the hidden features outputted by the second LSTM. Therefore, the final loss function is the combination of the regression loss and the transfer loss, which is denoted as,

$$\mathscr{L}=\mathscr{L}_{MSE}+\lambda\mathscr{L}_{MMD}, \tag{12}$$

where λ is the transfer loss weight, which represents the penalty coefficients to denote how much the domain adaptation needs to be considered. The transfer loss weight is set as 0.01 in this paper. In this way, the trained model could estimate the SoH or dT curve while considering the domain discrepancy between the source battery and the testing battery. The model is built by PyTorch, where the Adam optimizer is used to train the parameters of the neural networks.

4. Health prognostic results and discussion

The health prognostic results including the *dT* curve reconstruction and SoH estimation are presented and evaluated in this section according to the framework described above, where different testing scenarios are considered. To evaluate the accuracy of the prognostic results, the root mean square error (RMSE) and mean absolute error (MAE) are used, which are denoted as follows,

$$RMSE = \sqrt{\frac{1}{N}\sum_{i=1}^{N}(\hat{z}_i - z_i)^2}, \tag{13}$$

$$MAE = \frac{1}{N}\sum_{i=1}^{N}|\hat{z}_i - z_i|, \tag{14}$$

where $\hat{z}_i$ and z_i are the estimated value and real value for the i-th observation. The maximum absolute error (MaxAE) is also included in the performance evaluation. In the following subsections, the results for the *dT* curve reconstruction and SoH estimation are first presented and evaluated using the Lab datasets. Second, the generalization and robustness are evaluated by verifying the results on the two public datasets. Finally, further comparative evaluation and limitations are discussed.

4.1. DT curve reconstruction

The results for the *dT* curve reconstruction of the primary life battery aging under MCC fast charging and dynamic discharging and the second life battery aging under CC-CV charging and CC discharging are presented and evaluated. The results for the primarily used batteries under MCC fast charging and dynamic discharging are shown in Fig. 4. Fig. 4 (a)–(c) show the results of using cell 1 (UDDS) as the source battery and cell 2 (HWFET) as a target battery (denoted as "L#1_C1_to_C2"), while Fig. 4 (d)–(f) are the results considering the opposite scenario (denoted as "L#1_C1_to_C2"). Fig. 4(a) and (d) are the results obtained by the basic LSTM model while Fig. 4(b) and (e) are the results obtained by the DA-based LSTM, where the transfer loss is added in the total loss function for the parameter training, i.e. the proposed method. Fig. 4(c) and (f) show the peak values of the reconstructed *dT* curves and the real *dT* curve. Note that "Real", "Base", and "DA" in the figures represent the real curve, results obtained by the basic LSTM model, and the results obtained by the proposed domain adaptative method, respectively. It illustrates that the STS model by the LSTM can reconstruct the *dT* curve with the measured *dQ* curve in a scenario without the requirement of the temperature sensor. However, the trend of the reconstructed curve by the basic LSTM model still shows some obvious outliers, which is caused by the domain discrepancy between the training battery and the test battery. While the DA model shows better performances, the numerical comparison is given later below. The peak value of the *dT* curve is one significant feature for battery health prognostic and has a high correlation with the battery capacity [20,46]. It also shows that the proposed method could improve the accuracy of the estimations from the peak values of the *dT* curve.

The performance of the proposed method for the *dT* curve reconstruction under variable temperatures for the second-life batteries is also evaluated. The estimation results are shown in Fig. 5, where the interpretation of each subfigure is identical to that of Fig. 4. Under variable temperatures, the *dT* curves do not have monotonous trends for cycling from start to end because the correlation between the capacity and the environmental temperature also influences the shape of the degradation curves. Under this scenario, the reconstructed curves based on the proposed method have significant improvement compared to the basic LSTM method. Although the trends of the *dT* curve could be estimated by the basic LSTM, the curves show obvious differences from the real curves and the estimated peak values have large differences from the real values, which will negatively affect the SoH estimation. However, the reconstructed *dT* curves and the corresponding peak values found using the DA-based LSTM are much closer to the real values, which means that the information from the temperature variation could be extracted to help the health prognostic.

The numerical comparisons between the basic LSTM and the proposed DA-based LSTM are listed in Table 2 and Table 3, showing the errors of the reconstructed *dT* curve and the estimated peak values respectively. Note that the nomenclature for the test scenarios is defined as "Dataset_source battery_to_target battery". Significant improvements can be seen in the proposed method compared to the basic LSTM. The mean RMSE and MAE for the four testing scenarios of the basic LSTM for the *dT* curve reconstruction were 0.0854 °C/V and 0.0634 °C/V, respectively. While those for the proposed method are reduced to 0.0661 °C/V and 0.0491 °C/V, i.e. a reduction of 22.6%. Furthermore, the reduction in errors of the estimated peak values, when using the proposed method compared to the basic LSTM was 51.5% and 54.4% respectively. In addition, three generally used machine learning algorithms are also included for comparison of the STS *dT* estimation: artificial neural network (ANN), random forest (RF), and Gaussian process regression (GPR). It shows that the basic LSTM, RF, and GPR have similar accuracy and are better than ANN. Although one of them may perform better than the others on some batteries, it also performs worse than others on other batteries, which means the robustness of the conventional data-driven methods is not satisfactory. The mean error of the LSTM, RF, and GPR shows that LSTM is better for most cases but not significantly. All three methods could be used for the STS *dT* curve reconstruction conventionally, but the proposed DA-based LSTM method can improve the accuracy of the LSTM by accounting for the domain discrepancies and maintaining high accuracy in the different testing scenarios. The MaxAE for the reconstructed *dT* curves are listed

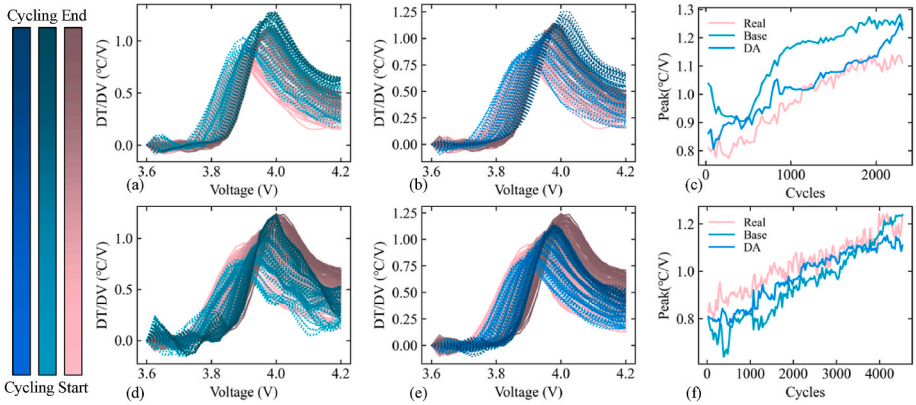

Fig. 4. The estimated *dT* curve and the peak values for Lab dataset#1.

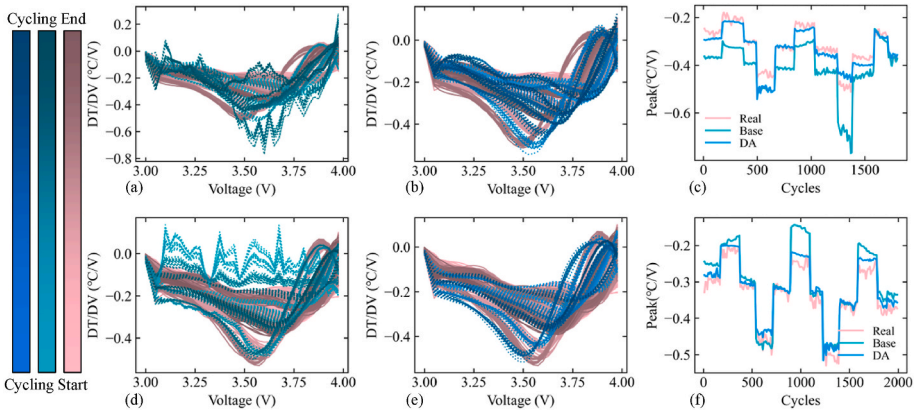

Fig. 5. The estimated *dT* curve and the peak values for Lab dataset#2.

Table 2
Comparative results of errors (°C/V) for the *dT* curve reconstruction based on different methods.

Test	LSTM		LSTM_DA		ANN		RF		GPR	
	RMSE	MAE	RMSE	MAE	RMSE	MAE	RMSE	MAE	RMSE	MAE
L#1_C1_to_C2	0.109	0.0834	0.0839	0.0625	0.113	0.0844	0.113	0.0944	0.0982	0.0747
L#1_C2_to_C1	0.106	0.0808	0.0879	0.0662	0.172	0.141	0.107	0.0804	0.123	0.0936
L#2_C1_to_C2	0.0827	0.0560	0.0504	0.0360	0.0855	0.0610	0.0782	0.0503	0.0786	0.0584
L#2_C2_to_C1	0.0437	0.0332	0.0420	0.0317	0.0635	0.0523	0.0627	0.0478	0.0576	0.0425
Mean	0.0854	0.0634	0.0661	0.0491	0.109	0.0847	0.0902	0.0682	0.0894	0.0673

Table 3
Errors (°C/V) of the estimated peak values.

Test	LSTM		LSTM_DA		ANN		RF		GPR	
	RMSE	MAE	RMSE	MAE	RMSE	MAE	RMSE	MAE	RMSE	MAE
L#1_C1_to_C2	0.139	0.127	0.0630	0.0512	0.159	0.157	0.126	0.113	0.0801	0.0681
L#1_C2_to_C1	0.107	0.0919	0.0662	0.0550	0.208	0.198	0.116	0.109	0.167	0.162
L#2_C1_to_C2	0.0897	0.0768	0.0306	0.0244	0.0724	0.0592	0.0619	0.0407	0.0622	0.0415
L#2_C2_to_C1	0.0391	0.0301	0.0218	0.0183	0.0507	0.0334	0.0687	0.0589	0.0674	0.0573
Mean	0.0937	0.0815	0.0454	0.0372	0.123	0.112	0.0932	0.0804	0.0942	0.0822

in Table 4, where the LSTM and proposed domain adaptative LSTM are compared. It shows that the mean MaxAE of the reconstructed *dT* curves for the four testing scenarios is 0.156 °C/V with basic LSTM while is 0.100 °C/V with the proposed method. The MaxAE for the peak value between the reconstructed *dT* curve and the real curve is 0.218 °C/V and 0.117 °C/V based on the basic LSTM and the domain adaptative LSTM, respectively. Both of the results indicate that the proposed method improves the accuracy of the *dT* curve reconstruction. Therefore, it is illustrated from the comparative results that the proposed method has better accuracy and robustness than the conventional data-driven methods.

Table 4
Comparisons of the maximum absolute errors (°C/V) for the *dT* curve reconstruction.

Test	LSTM		LSTM_DA	
	Curve	Peack value	Curve	Peack value
L#1_C1_to_C2	0.125	0.279	0.111	0.157
L#1_C2_to_C1	0.155	0.230	0.136	0.169
L#2_C1_to_C2	0.233	0.261	0.0904	0.0899
L#2_C2_to_C1	0.111	0.101	0.0642	0.0535
Mean	0.156	0.218	0.100	0.117

4.2. SoH estimation

The SoH estimation results of the two Lab datasets are presented and evaluated in this section. Due to the different working conditions, the degradation of the two batteries in the two datasets shows significant differences with different degradation rates and lifespans.

The estimations for the primary batteries aging under HWFET and UDDS discharging with MCC fast charging are shown in Fig. 6(a)-(b) and Fig. 6(c)–(d), respectively. The SoH estimation results obtained with the basic LSTM reconstructed *dT* curve, and DA-based LSTM reconstructed *dT* curve but without DA for the SoH model are also presented for the comparisons, referred to as “Benchmark 1” and “Benchmark 2”, respectively. The proposed method in the figures is a two-stage DA process, which is denoted as the “Multi DA”. The SoH is normalized by dividing the first value because of the manufactural inconsistency. It shows above that when the DA-based model is used for *dT* curve reconstruction, more accurate temperature variation information could be obtained. Therefore, an obvious improvement from the results obtained from “Benchmark 1” to “Benchmark 2” can be seen in Fig. 6, where a more linear correlation is shown for the figure of estimated SoH to the real SoH. The numerical results of the estimation errors for the SoH are shown in Table 4. It illustrates that the RMSE and MAE are reduced from 3.317% to 3.123%–1.687% and 1.524% for cell 2, and 2.241% and 1.828%–1.756% and 1.573% for cell 1 respectively from the ”Benchmark 1” to “Benchmark 2”. When the DA is also used in the SoH estimation model, the estimated results are improved, as the RMSE

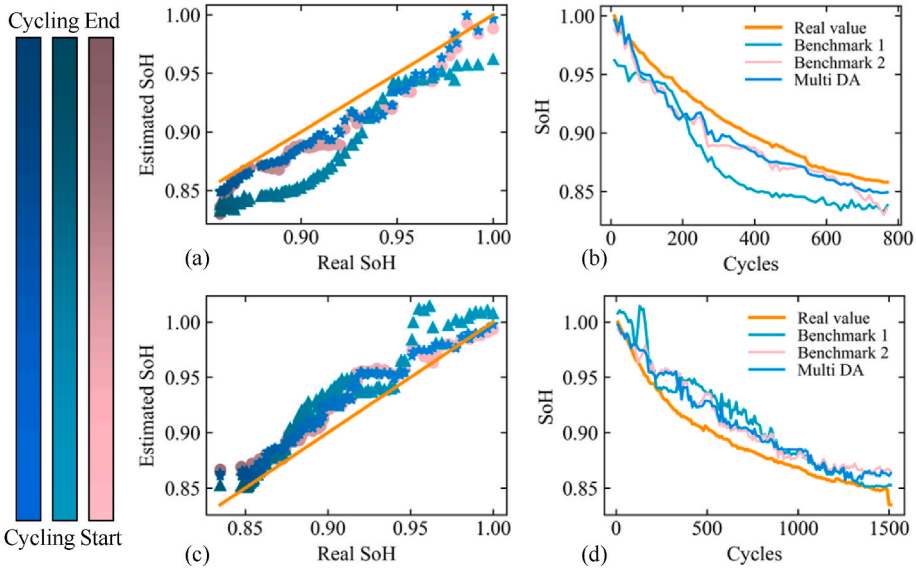

Fig. 6. SoH estimation results for Lab dataset #1. (a)/(b) The estimation results for cell 2 with cell 1 as the source battery, (c)/(d) The estimation results for cell 1 with cell 2 as the source battery.

and MAE are reduced to 1.364% and 1.257% for cell 2, and 1.671% and 1.519% for cell 1, respectively. Therefore, it indicates from the evaluation of the results above that the multi-DA processes using only unlabeled data help improve the health prognostic for batteries compared to the basic LSTM without domain adaptation.

The SoH estimations for the second-life batteries aging under cyclic environmental temperatures are also presented and evaluated. The estimation results for cell 2 and cell 1 are shown in Fig. 7(a)-(b) and Fig. 7(c)–(d), respectively. Note that the jumps shown in the SoH curves are caused by the temperature changes since the charged/discharged capacity under different temperatures is different. Also, two benchmarks are used for the comparisons, which should be interpreted the same way above. The results in Fig. 7(b) and (d) clearly demonstrate the convergence of the real values from "Benchmark 1" to "Benchmark 2" to the "Multi-DA", improving the accuracy with each step. The results in Fig. 7 (a) and (c) show that although linear correlation exists between the estimated SoH and the real SoH for "Benchmark 1" and "Benchmark 2", they diverge from the one-to-one line, implying a divergence between the estimated and real values. While the estimated SoH of the proposed method shows very little divergence indicating a satisfactory linear correlation. The colors of the dots in Fig. 7(a) and (c) do not show the monotonic variations and the dots have discontinuous blanks because the capacity also changes with environmental temperatures. The numerical results shown in Table 4 clearly show the accuracy improvement of the proposed method. It illustrates that "Benchmark 1" has the largest estimation errors compared to "Benchmark 2" and the multi-DA method. The RMSE and MAE of "Benchmark 1" in the two are even larger than 4%, which are significantly reduced to less than 2.1% by the proposed multi-DA method. The errors of "Benchmark 2" are also less than those of "Benchmark 1", but still larger than that of the proposed multi-DA method. This indicates that the DA-based dT curve reconstruction could provide more accurate temperature variation information to improve the SoH estimation accuracy, and the second DA in the SoH estimation model reduces domain discrepancy of the hidden features for

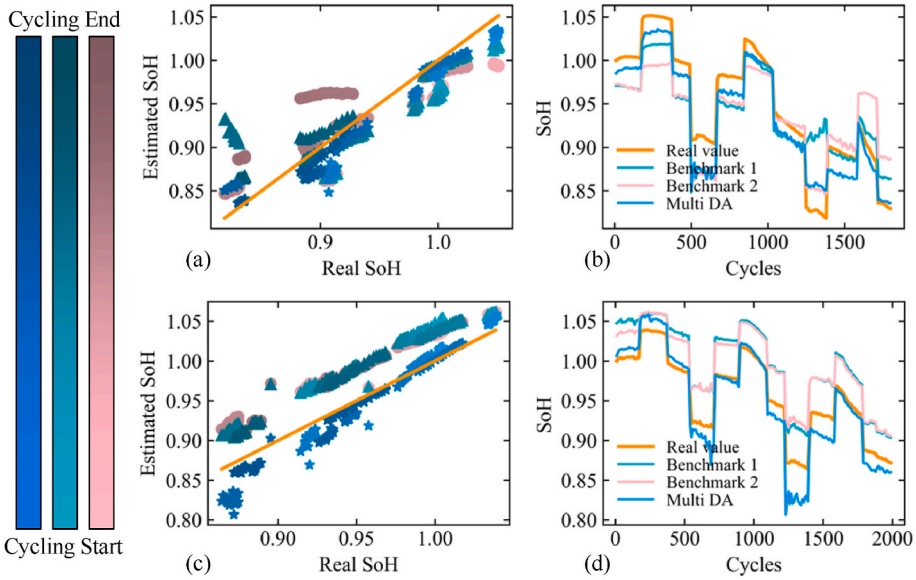

Fig. 7. SoH estimation results for Lab dataset #2. (a)/(b) The estimation results for cell 2 with cell 1 as the source battery, (c)/(d) The estimation results for cell 1 with cell 2 as the source battery.

the SoH estimation between the source and target domain, which therefore further improves the SoH estimation.

The mean RMSE, MAE, and MaxAE for the four testing scenarios are also shown in Table 5. It shows that "Benchmark 1" has the largest errors, whose RMSE and MAE are 3.344% and 3.038% respectively. The errors are reduced to 2.750% and 2.482% i.e., an error reduction of 17.763% and 18.302%, with the improved *dT* curve reconstruction to provide better temperature information. When the DA is also used for the SoH estimation, the RMSE and MAE are reduced to 1.772% and 1.532%, respectively. Therefore, the RMSE and MAE have been reduced by 47.010% and 49.572% respectively from "Benchmark 1" to the proposed method for battery SoH estimation under variable temperatures. The reduction trend also shows in the results of MaxAE, indicating the accuracy improvement of the proposed method compared to benchmarks, which reduced from 7.340% to 4.689%. The results indicate the effectiveness of the proposed end-to-end multi-DA method for battery health prognostic with *dT* curve reconstruction and SoH estimation.

Although it has been verified in published works that the information of *dT* curve could help improve the accuracy of battery SoH estimation, this paper also proves that under variable temperature conditions. To demonstrate the effectiveness of the *dT* information on the SoH estimation, the comparisons between the proposed method and the ones without *dT* information are presented in Table 6. "Benchmark without *dT*" refers to the model trained by only using *dQ* information and is directly used for the SoH estimation of the test batteries. "DA without *dT*" means the above model with DA for the SoH estimation. It shows that although the DA could improve the accuracy of the model compared to "Benchmark without *dT*", the additional *dT* information provides more accurate estimations, especially with two stages of DA. The results illustrate that the temperature variation information provided by the *dT* curve helps improve the SoH estimation, which is because the capacity also varies with temperatures. In real applications, the environmental temperatures also change with the seasons. Therefore, the additional temperature information provided by the reconstructed *dT* curve based on the proposed prognostic method could not only provide thermal behavior monitoring but also help improve the estimation of SoH.

4.3. Robustness evaluation with different manufactory

The results above have verified the prognostics under more practical scenarios, which are fast charging with dynamic discharging and variable temperature conditions. In this section, the public datasets are also used for verification to evaluate the robustness of the proposed method. The first two batteries from the Ox data set, whose current rate is much smaller than the Lab datasets with smaller temperature variations, will be used for demonstration. The estimation results are shown in Fig. 8, where Fig. 8(a)–8(c) are the results for cell 2 while Fig. 8(d)–8(f) are the results for cell 1 with the other battery serving as the source battery. The estimation results for the *dT* curve based on the proposed method, the error for the peak value, and the SoH estimation results based on the proposed method and two benchmarks are given. The peak value here refers to the valley, which is still presented as the peak value to make the presentation consistent across the entire paper. The numerical results of the *dT* curve reconstruction are listed in Table 7. It shows that the variation of the *dT* curve could be estimated satisfactorily with RMSE and MAE less than 0.018 °C/V and 0.013 °C/V, respectively. The MaxAE is less than 0.026 °C/V for all the testing scenarios while the mean MaxAE for those results based on the basic LSTM is 0.045 °C/V. The proposed multi-DA SoH estimation method is also more accurate than the two benchmarks. The results obtained by the DA estimated *dT* curve are more accurate than the most conventional method, i.e., "Benchmark 1". The RMSE, MAE, and MaxAE of the SoH estimations for the proposed method are less than 1.46%, 1.04%, and 4.07% respectively as listed in Table 8. It shows that the MaxAE is not reduced significantly, because the largest errors come from the estimations of some deviation points as shown in Fig. 8. But the overall estimations based on the proposed method are better converged to the real values.

Table 6
SoH estimate errors (%) for the experimental batteries.

Method	L#2_C1_to_C2		L#2_C2_to_C1	
	RMSE	MAE	RMSE	MAE
Benchmark without *dT*	3.738	3.478	3.984	3.919
DA without *dT*	2.647	1.999	3.262	2.901
Benchmark with *dT*	3.649	3.011	3.907	3.819
Multi DA	2.091	1.842	1.961	1.511

Finally, two batteries from MIT-Stanford data sets are used for the verification. The "channel id" of the two batteries are 25 and 29 respectively, whose lifetimes are 1638 and 1115 cycles, respectively. The estimation results are also shown in Table 7 for the *dT* curve reconstruction and in Table 8 for the SoH estimation, respectively. The results show the accuracy improvement from "Benchmark 1" to "Benchmark 2" and to the proposed method. The RMSE and MAE for the *dT* curve reconstructions are less than 0.013 °C/V and 0.0085 °C/V respectively while those for SoH estimation are less than 0.92% and 0.72% of the proposed multi-DA method. The mean values of the four testing scenarios using the public data sets are also listed in Tables 7 and 8. The results show that the RMSE and MAE for the *dT* curve reconstruction have been reduced from 0.0187 °C/V and 0.0127 °C/V to 0.0132 °C/V and 0.00954 °C/V, with the reduction percentages of 29.412% and 24.882% respectively. The results show that the RMSE and MAE for the SoH estimation have been reduced from 1.502% and 1.084% to 1.045% and 0.815% respectively, with reduction percentages of 30.519% and 24.815% respectively. Therefore, the verification by the two public datasets also demonstrates the effectiveness of the proposed method for battery health prognostics and the performance improvement compared to the basic LSTM-based method.

4.4. Discussion

This paper proposes a novel and more comprehensive battery health prognostic method to provide the estimation of both *dT* curve variation and battery SoH. The experimental data sets are collected from the aging test that is closer to the real world and the full life span test is conducted. From the results presented and discussed above, it can be summarized that DA is a good way to make better use of the unlabeled data from the target domain to improve the prognostic accuracy. Two public data sets are used to verify the effectiveness of the proposed method under

Table 5
SoH estimate errors (%) for the experimental batteries.

Test	Benchmark 1			Benchmark 2			Multi DA		
	RMSE	MAE	MaxAE	RMSE	MAE	MaxAE	RMSE	MAE	MaxAE
L#1_C1_to_C2	3.317	3.123	4.807	1.687	1.524	3.218	1.364	1.257	2.816
L#1_C2_to_C1	2.241	1.828	5.687	1.756	1.573	3.649	1.671	1.519	3.525
L#2_C1_to_C2	3.717	3.180	11.330	3.649	3.011	7.344	2.091	1.842	5.896
L#2_C2_to_C1	4.102	4.021	7.534	3.907	3.819	7.621	1.961	1.511	6.519
Mean	3.344	3.038	7.340	2.750	2.482	5.458	1.772	1.532	4.689

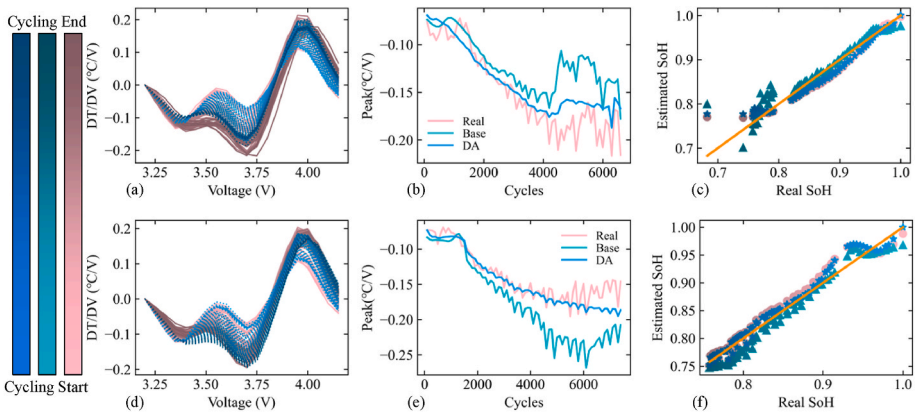

Fig. 8. SoH estimation results for the Oxford dataset 2. (a)/(b) The estimation results for cell 2 with cell 1 as the source battery, (c)/(d) The estimation results for cell 1 with cell 2 as the source battery.

Table 7
Errors (°C/V) of the estimated *dT* curves and the peak values for the public datasets.

Test	Errors of the estimated *dT* curve						Errors of the estimated *dT* peak value					
	LSTM			LSTM_DA			LSTM			LSTM_DA		
	RMSE	MAE	MaxAE	RMSE	MAE	MaxAE	RMSE	MAE	MaxAE	RMSE	MAE	MaxAE
Ox_C1_to_C2	0.0268	0.0172	0.0926	0.0180	0.0129	0.0345	0.0376	0.0292	0.0873	0.0219	0.0165	0.0496
Ox _C2_to_C1	0.0244	0.0172	0.0338	0.0150	0.0111	0.0258	0.0452	0.0371	0.0883	0.0154	0.0108	0.0409
MS_C1_to_C2	0.0123	0.00845	0.0321	0.0103	0.00738	0.0226	0.0196	0.0165	0.0611	0.0167	0.0143	0.0488
MS_C2_to_C1	0.0113	0.00783	0.0215	0.00976	0.00676	0.0196	0.0190	0.0164	0.0456	0.0147	0.0115	0.0391
Mean	0.0187	0.0127	0.0450	0.0132	0.00954	0.0256	0.0304	0.0248	0.0706	0.0172	0.0133	0.0446

Table 8
SoH estimate errors (%) for the public datasets.

Test	Benchmark 1			Benchmark 2			Multi DA		
	RMSE	MAE	MaxAE	RMSE	MAE	MaxAE	RMSE	MAE	MaxAE
Ox_C1_to_C2	2.365	1.466	11.737	1.786	1.361	8.787	1.654	1.239	9.073
Ox _C2_to_C1	1.631	1.333	3.465	1.421	1.241	3.423	1.172	0.969	3.493
MS_C1_to_C2	0.941	0.772	2.187	0.686	0.585	1.683	0.641	0.537	1.549
MS_C2_to_C1	1.072	0.765	2.622	0.942	0.823	2.364	0.911	0.714	2.131
Mean	1.502	1.084	5.003	1.209	1.003	4.064	1.045	0.815	4.062

different application scenarios. In order to further demonstrate the improvement of the *dT* curve reconstruction and SoH estimation with the multi-DA processes, the comparative results of the RMSE and MAE for the *dT* curve and *dT* curve peak estimations based on the base model and the DA model are shown in Fig. 9(a). The comparisons between the Multi DA-based SoH estimation and two benchmarks are shown in Fig. 9 (b). The box plots clearly illustrate the error reduction for the *dT* curve reconstruction by the proposed DA method compared to the basic LSTM model. In addition, the error distributions of the proposed method are also much narrower for the multi-DA method, which means the generalization and robustness of the proposed method are also better than the conventional data-driven method.

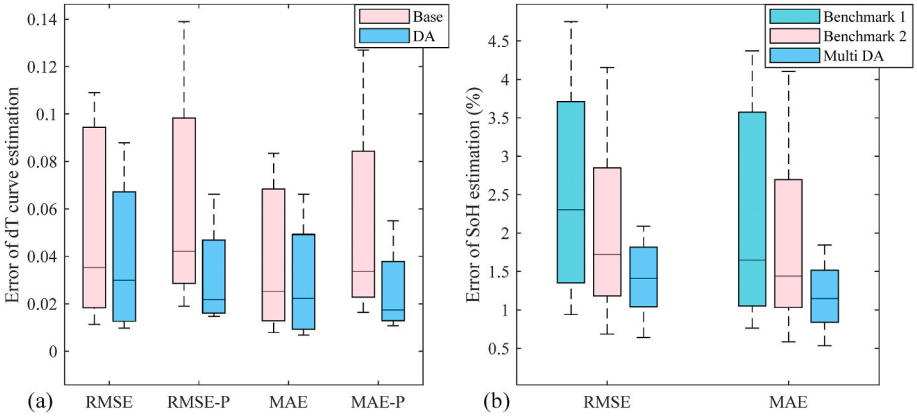

Fig. 9. Comparative evaluations of the *dT* curve and SoH estimations.

However, there are still some limitations. For example, the *dT* curve and *dQ* curve vary with the current rate, which makes it difficult to reconstruct the *dT* curve when the batteries work under different charging loads. While the method proposed in this paper could cover the prognostic under the same charging or discharging profile but with different aging degradation patterns, further research is needed to get accurate prognostics under different *dT* shapes. Although different voltage ranges have been selected for the demonstration of the effectiveness of the proposed strategy and satisfactory results have been obtained under the ultra-fast charging stage with 10C (Lab dataset #1), the continuously sampled data are used. In practical applications, the sampling frequency is much smaller with some missing data. Therefore, the *dT* curve reconstruction and SoH estimation with discontinuously sampled data are valuable for studying in the future. In addition, a battery pack will have an inconsistent temperature distribution, i.e. connected battery cells will have different temperature variations. Therefore, the prognostic for the battery pack and its connected battery cells also needs further research. The experimental result in this paper has been a good example of more comprehensive health prognostics considering both temperature and capacity variation estimations. For example, in EVs or smart grids, the charging schedule keeps the same despite the different dynamic discharging profiles or variable temperatures, the results using the Lab datasets have proved the effectiveness of the proposed method in those application scenarios.

5. Conclusion

Battery health prognostics are a key component of battery management systems for predictive maintenance of electrified transportation. Both temperature variation and capacity fade are significant for monitoring safe operation. This paper proposed one novel end-to-end method with multi-DA for sensor-free *dT* curve reconstruction and SoH estimation using *Q-V* data. To improve the accuracy and generalization, DA is integrated into the hidden layers to reduce the domain discrepancy. In SoH estimation, the reconstructed *dT* curve is added to provide information on temperature variation as an input, and another DA is adopted to further reduce the domain discrepancy of the hidden features for the SoH estimation.

Battery aging test for the whole life span is conducted, which includes both primary life and second life testing. The estimation results for the *dT* curve have proved that the proposed method brings more than 20% error reduction compared to the conventional methods without domain adaptation. The estimation accuracy for SoH estimation could be improved by the reconstrued *dT* curve with error reductions of 17.763% and 18.302% for the RMSE and MAE, respectively compared to the basic model only using IC curve. When the DA is also adapted to the SoH estimation, the RMSE and MAE can be reduced by 47.010% and 49.572%, respectively. Furthermore, two public datasets were also used in this paper for generalization verification.

Only unlabeled data of the testing batteries are used, which broadens the transfer learning strategies for prognostic performance improvement. The proposed strategy is promising to be implemented considering various applications according to the satisfactory testing results under different scenarios. Moreover, different prognostic tasks can also be integrated into this framework by considering multi-task learning for more practical requirements, which will be studied in future work.

CRediT authorship contribution statement

Yunhong Che: Conceptualization, Methodology, Software, Investigation, Visualization, Writing – original draft. **Søren Byg Vilsen:** Methodology, Writing – original draft, Writing – review & editing. **Jinhao Meng:** Validation, Writing – original draft, Writing – review & editing. **Xin Sui:** Writing – review & editing. **Remus Teodorescu:** Supervision, Project administration, Funding acquisition.

Declaration of competing interest

The authors declare that they have no known competing financial interests or personal relationships that could have appeared to influence the work reported in this paper.

Data availability

The data that has been used is confidential.

Acknowledgment

This research was funded by the “SMART BATTERY” project, granted by Villum Foundation in 2021 (project number 222860).

References

[1] Han X, Lu L, Zheng Y, Feng X, Li Z, Li J, et al. A review on the key issues of the lithium ion battery degradation among the whole life cycle. ETransportation 2019;1:100005. https://doi.org/10.1016/j.etran.2019.100005.
[2] Song Z, Yang XG, Yang N, Delgado FP, Hofmann H, Sun J. A study of cell-to-cell variation of capacity in parallel-connected lithium-ion battery cells. ETransportation 2021;7:100091. https://doi.org/10.1016/j.etran.2020.100091.
[3] Che Y, Deng Z, Lin X, Hu L. Predictive battery health management with transfer learning and online model correction. IEEE Trans Veh Technol 2021;70:1269–77.
[4] Ren D, Hsu H, Li R, Feng X, Guo D, Han X, et al. A comparative investigation of aging effects on thermal runaway behavior of lithium-ion batteries. ETransportation 2019;2:100034. https://doi.org/10.1016/j.etran.2019.100034.
[5] Che Y, Deng Z, Li P, Tang X, Khosravinia K, Lin X, et al. State of health prognostics for series battery packs: a universal deep learning method. Energy 2022;238:121857. https://doi.org/10.1016/j.energy.2021.121857.
[6] Xiong R, Li L, Tian J. Towards a smarter battery management system: a critical review on battery state of health monitoring methods. J Power Sources 2018;405:18–29. https://doi.org/10.1016/j.jpowsour.2018.10.019.
[7] Shi H, Wang S, Wang L, Xu W, Fernandez C, Dablu BE, et al. On-line adaptive asynchronous parameter identification of lumped electrical characteristic model for vehicle lithium-ion battery considering multi-time scale effects. J Power Sources 2022;517:230725. https://doi.org/10.1016/j.jpowsour.2021.230725.
[8] Shi H, Wang L, Wang S, Fernandez C, Xiong X, Dablu BE, et al. A novel lumped thermal characteristic modeling strategy for the online adaptive temperature and parameter co-estimation of vehicle lithium-ion batteries. J Energy Storage 2022;50:104309. https://doi.org/10.1016/j.est.2022.104309.
[9] Sun J, Tang C, Li X, Wang T, Jiang T, Tang Y, et al. A remaining charging electric quantity based pack available capacity optimization method considering aging inconsistency. ETransportation 2022;11:100149. https://doi.org/10.1016/j.etran.2021.100149.
[10] Liu W, Hu X, Lin X, Yang X, Song Z, Foley AM, et al. Toward high-accuracy and high-efficiency battery electrothermal modeling : a general approach to tackling modeling errors. ETransportation 2022;14:100195. https://doi.org/10.1016/j.etran.2022.100195.
[11] Hu X, Che Y, Lin X, Deng Z. Health prognosis for electric vehicle battery packs: a data-driven approach. IEEE/ASME Trans Mechatronics 2020;25:2622–32. https://doi.org/10.1109/TMECH.2020.2986364.
[12] Lai X, Chen Q, Tang X, Zhou Y, Gao F, Guo Y, et al. Critical review of life cycle assessment of lithium-ion batteries for electric vehicles: a lifespan perspective. ETransportation 2022;12:100169. https://doi.org/10.1016/j.etran.2022.100169.
[13] Che Y, Foley A, El-Gindy M, Lin X, Hu X, Pecht M. Joint estimation of inconsistency and state of health for series battery packs. Automot Innov 2021;4:103–16. https://doi.org/10.1007/s42154-020-00128-8.
[14] Meng J, Cai L, Stroe DI, Huang X, Peng J, Liu T, et al. An automatic weak learner formulation for lithium-ion battery state of health estimation. IEEE Trans Ind Electron 2022;69:2659–68. https://doi.org/10.1109/TIE.2021.3065594.
[15] Zhu J, Wang Y, Huang Y, Bhushan Gopaluni R, Cao Y, Heere M, et al. Data-driven capacity estimation of commercial lithium-ion batteries from voltage relaxation. Nat Commun 2022;13:1–10. https://doi.org/10.1038/s41467-022-29837-w.
[16] Vilsen SB, Stroe DI. Battery state-of-health modelling by multiple linear regression. J Clean Prod 2021;290:125700. https://doi.org/10.1016/j.jclepro.2020.125700.
[17] Su L, Wu M, Li Z, Zhang J. Cycle life prediction of lithium-ion batteries based on data-driven methods. ETransportation 2021;10:100137. https://doi.org/10.1016/j.etran.2021.100137.
[18] Rauf H, Khalid M, Arshad N. Machine learning in state of health and remaining useful life estimation: theoretical and technological development in battery degradation modelling. Renew Sustain Energy Rev 2022;156:111903. https://doi.org/10.1016/j.rser.2021.111903.
[19] She C, Zhang L, Wang Z, Sun F, Liu P, Song C. Battery state of health estimation based on incremental capacity analysis method: synthesizing from cell-level test to real-world application. IEEE J Emerg Sel Top Power Electron 2021:1. https://doi.org/10.1109/JESTPE.2021.3112754.
[20] Tian J, Xiong R, Shen W. State-of-Health estimation based on differential temperature for lithium ion batteries. IEEE Trans Power Electron 2020;35:10363–73. https://doi.org/10.1109/TPEL.2020.2978493.

[21] Greenbank S, Howey D. Automated feature extraction and selection for data-driven models of rapid battery capacity fade and end of life. IEEE Trans Ind Inf 2022;18:2965–73. https://doi.org/10.1109/TII.2021.3106593.
[22] Hu X, Che Y, Lin X, Onori S. Battery health prediction using fusion-based feature selection and machine learning. IEEE Trans Transp Electrif 2021;7:382–98. https://doi.org/10.1109/TTE.2020.3017090.
[23] Shen S, Sadoughi M, Li M, Wang Z, Hu C. Deep convolutional neural networks with ensemble learning and transfer learning for capacity estimation of lithium-ion batteries. Appl Energy 2020;260:114296. https://doi.org/10.1016/j.apenergy.2019.114296.
[24] Li W, Sengupta N, Dechent P, Howey D, Annaswamy A, Sauer DU. One-shot battery degradation trajectory prediction with deep learning. J Power Sources 2021;506:230024. https://doi.org/10.1016/j.jpowsour.2021.230024.
[25] Ren L, Dong J, Wang X, Meng Z, Zhao L, Deen MJ. A data-driven auto-CNN-LSTM prediction model for lithium-ion battery remaining useful life. IEEE Trans Ind Inf 2021;17:3478–87. https://doi.org/10.1109/TII.2020.3008223.
[26] Che Y, Deng Z, Tang X, Lin X, Nie X, Hu X. Lifetime and aging degradation prognostics for lithium-ion battery packs based on a cell to pack method. Chin J Mech Eng 2022;35. https://doi.org/10.1186/s10033-021-00668-y.
[27] Tian J, Xiong R, Shen W, Lu J, Yang XG. Deep neural network battery charging curve prediction using 30 points collected in 10 min. Joule 2021;5:1521–34. https://doi.org/10.1016/j.joule.2021.05.012.
[28] Gong Q, Wang P, Cheng Z. An encoder-decoder model based on deep learning for state of health estimation of lithium-ion battery. J Energy Storage 2022;46:103804. https://doi.org/10.1016/j.est.2021.103804.
[29] Tang X, Gao F, Lai X. Compressing and reconstructing the voltage data for lithium-ion batteries using model migration and un-equidistant sampling techniques. ETransportation 2022;13:100186. https://doi.org/10.1016/j.etran.2022.100186.
[30] Che Y, Zheng Y, Wu Y, Sui X, Bharadwaj P, Stroe D, et al. Data efficient health prognostic for batteries based on sequential information-driven probabilistic neural network. Appl Energy 2022;323:119663. https://doi.org/10.1016/j.apenergy.2022.119663.
[31] Han T, Wang Z, Meng H. End-to-end capacity estimation of Lithium-ion batteries with an enhanced long short-term memory network considering domain adaptation. J Power Sources 2022;520:230823. https://doi.org/10.1016/j.jpowsour.2021.230823.
[32] Tian J, Xiong R, Shen W, Sun F. Electrode ageing estimation and open circuit voltage reconstruction for lithium ion batteries. Energy Storage Mater 2021;37:283–95. https://doi.org/10.1016/j.ensm.2021.02.018.
[33] Tang X, Wang Y, Liu Q, Gao F. Reconstruction of the incremental capacity trajectories from current-varying profiles for lithium-ion batteries. iScience 2021;24:103103. https://doi.org/10.1016/j.isci.2021.103103.
[34] Li X, Yuan C, Wang Z, He J, Yu S. Lithium battery state-of-health estimation and remaining useful lifetime prediction based on non-parametric aging model and particle filter algorithm. ETransportation 2022;11:100156. https://doi.org/10.1016/j.etran.2022.100156.
[35] Ojo O, Lang H, Kim Y, Hu X, Mu B, Lin X. A neural network based method for thermal fault detection in lithium-ion batteries. IEEE Trans Ind Electron 2021;68:4068–78. https://doi.org/10.1109/TIE.2020.2984980.
[36] Zhu S, He C, Zhao N, Sha J. Data-driven analysis on thermal effects and temperature changes of lithium-ion battery. J Power Sources 2021;482:228983. https://doi.org/10.1016/j.jpowsour.2020.228983.
[37] Oxford battery degradation. Dataset 1, https://ora.ox.ac.uk/objects/uuid:03ba4b01-cfed-46d3-9b1a-7d4a7bdf6fac; 2017.
[38] Severson KA, Attia PM, Jin N, Perkins N, Jiang B, Yang Z, et al. Data-driven prediction of battery cycle life before capacity degradation. Nat Energy 2019;4:383–91. https://doi.org/10.1038/s41560-019-0356-8.
[39] Liu K, Shang Y, Ouyang Q, Widanage WD. A data-driven approach with uncertainty quantification for predicting future capacities and remaining useful life of lithium-ion battery. IEEE Trans Ind Electron 2021;68:3170–80. https://doi.org/10.1109/TIE.2020.2973876.
[40] Tan Y, Zhao G. Transfer learning with long short-term memory network for state-of-health prediction of lithium-ion batteries. IEEE Trans Ind Electron 2020;67:8723–31. https://doi.org/10.1109/TIE.2019.2946551.
[41] Tian J, Xiong R, Shen W. A review on state of health estimation for lithium ion batteries in photovoltaic systems. ETransportation 2019;2:100028. https://doi.org/10.1016/j.etran.2019.100028.
[42] Che Y, Hu X, Lin X, Guo J, Teodorescu R. Health prognostics for lithium-ion batteries: mechanisms, methods, and prospects. Energy Environ Sci 2023. https://doi.org/10.1039/d2ee03019e.
[43] Wang S, Miao H, Li J, Cao J. Spatio-temporal knowledge transfer for urban crowd flow prediction via deep attentive adaptation networks. IEEE Trans Intell Transport Syst 2022;23:4695–705. https://doi.org/10.1109/TITS.2021.3055207.
[44] Ghifary M, Bastiaan Kleijn W, Zhang M. Domain adaptive neural networks for object recognition. Lect Notes Comput Sci 2014;8862:898–904. https://doi.org/10.1007/978-3-319-13560-1.
[45] Tzeng E, Hoffman J, Zhang N, Saenko K, Darrell T. Deep domain confusion: maximizing for domain invariance. 2014.
[46] Li X, Yuan C, Wang Z, Xie J. A data-fusion framework for lithium battery health condition Estimation Based on differential thermal voltammetry. Energy 2022;239:122206. https://doi.org/10.1016/j.energy.2021.122206.